

(January 1998)  
 TMUP-HEL-9801  
 UM-P-98/04  
 RCHEP-98/01

## Comparing and contrasting the $\nu_\mu \rightarrow \nu_\tau$ and $\nu_\mu \rightarrow \nu_s$ solutions to the atmospheric neutrino problem with SuperKamiokande data

R. Foot and R. R. Volkas  
*School of Physics*

*Research Centre for High Energy Physics*  
*The University of Melbourne*  
*Parkville 3052 Australia*

(*foot@physics.unimelb.edu.au, r.volkas@physics.unimelb.edu.au*)

O. Yasuda

*Department of Physics*  
*Tokyo Metropolitan University*

*1-1 Minami-Osawa Hachioji, Tokyo 192-03, Japan*  
 (*yasuda@phys.metro-u.ac.jp*)

### Abstract

The  $\nu_\mu \rightarrow \nu_\tau$  and  $\nu_\mu \rightarrow \nu_s$  solutions to the atmospheric neutrino problem are compared with SuperKamiokande data. The differences between these solutions due to matter effects in the Earth are calculated for the ratio of  $\mu$ -like to  $e$ -like events and for up-down flux asymmetries. These quantities are chosen because they are relatively insensitive to theoretical uncertainties in the overall neutrino flux normalisation and detection cross-sections and efficiencies. A  $\chi^2$  analysis using these quantities is performed yielding  $3\sigma$  ranges which are approximately given by  $(0.725 - 1.0, 4 \times 10^{-4} - 2 \times 10^{-2} \text{ eV}^2)$  and  $(0.74 - 1.0, 1 \times 10^{-3} - 2 \times 10^{-2} \text{ eV}^2)$  for  $(\sin^2 2\theta, \Delta m^2)$  for the  $\nu_\mu \rightarrow \nu_\tau$  and  $\nu_\mu \rightarrow \nu_s$  solutions, respectively. Values of  $\Delta m^2$  smaller than about  $2 \times 10^{-3} \text{ eV}^2$  are disfavoured for the  $\nu_\mu \rightarrow \nu_s$  solution, suggesting that future long baseline experiments should see a positive signal if this scenario is the correct one.

Atmospheric neutrino data provides important evidence for the existence of neutrino oscillations [1,2]. Atmospheric neutrinos are produced primarily from the decays of mesons and muons which result from interactions between the primary cosmic ray flux and air molecules in the Earth's upper atmosphere. The neutrino flux consists mostly of  $\nu_e$ ,  $\bar{\nu}_e$ ,  $\nu_\mu$  and  $\bar{\nu}_\mu$ , with the muon flavour flux expected to be roughly twice as large as the electron flavour flux. When these neutrinos interact with matter via the charged current they produce the corresponding charged leptons or antileptons. Atmospheric neutrino experiments measure the corresponding event rates. Historically, the atmospheric neutrino anomaly has been defined to be the discrepancy between measured values of the ratio of  $\mu$ -like to  $e$ -like events ( $\sim 1.2$ ) to the predicted ratio of about 2. The SuperKamiokande experiment has recently produced relatively high statistics data that considerably strengthens the case for an atmospheric neutrino anomaly [2]. In particular, the new data provide strong evidence for an anomalous zenith-angle dependence for multi-GeV  $\mu$ -like events. Furthermore, the pattern of this dependence is consistent with a neutrino oscillation explanation.

Generically, the atmospheric neutrino anomaly points for its solution towards large angle  $\nu_\mu \rightarrow \nu_e$  [3],  $\nu_\mu \rightarrow \nu_\tau$  [4] or  $\nu_\mu \rightarrow \nu_s$  [5] oscillations, where  $\nu_s$  denotes a sterile neutrino [6]. However,  $\nu_\mu \rightarrow \nu_e$  is now disfavoured (though not completely ruled out) by results from the CHOOZ reactor-based  $\bar{\nu}_e$  disappearance experiment [7]. We therefore focus on the  $\nu_\mu \rightarrow \nu_\tau$  and  $\nu_\mu \rightarrow \nu_s$  possibilities in this paper. A major goal of future atmospheric neutrino research should be to discriminate between these rival solutions. To this end, the purpose of this paper is to compare and contrast these two most favoured oscillation modes with the latest SuperKamiokande data.

Though in many respects similar, the  $\nu_\mu \rightarrow \nu_\tau$  and  $\nu_\mu \rightarrow \nu_s$  cases are distinguishable, because  $\nu_\tau$  interacts via the neutral current with ordinary matter whereas  $\nu_s$ , by definition, does not. Neutral current interactions with the Earth affect the evolution of the  $\nu_\mu + \nu_s$  system because of the matter effect [8]. The evolution of the  $\nu_\mu + \nu_\tau$  system is, by contrast, identical to what it would be in vacuum. A major goal of this paper is study the magnitude of the matter effect. We will show that it is quite important for multi-GeV events if  $\Delta m^2 < 10^{-2}$  eV<sup>2</sup> and for sub-GeV events if  $\Delta m^2 < 10^{-3}$  eV<sup>2</sup>. We will also perform a  $\chi^2$  analysis of the two cases with respect to the SuperKamiokande data. It is interesting to note that other ways of discriminating between  $\nu_\tau$  and  $\nu_s$  have been suggested in the literature. Reference [9] discusses how the sensitivity of SuperKamiokande to neutral current interactions can be used, while Ref. [10] discusses the importance of the matter effect for high energy neutrinos that produce upward-going muons. Intriguingly, the MACRO experiment [11] sees dips in the upward-going muon flux at zenith angles that are qualitatively consistent with expectations from Ref. [10]. The two cases may also be distinguished in the future using long baseline experiments, either through the sensitivity of the detector to neutral currents, or, for higher energy experiments, by searching for  $\nu_\tau$  appearance.

In the water-Cerenkov SuperKamiokande experiment, neutrinos are detected via the charged leptons  $\alpha$  ( $\alpha = e$  or  $\mu$ ) produced from neutrino scattering off nucleons in the water molecules:  $\nu_\alpha N \rightarrow \alpha X$ , where the identity of  $X$  will be discussed below. The total number  $N(\alpha)$  of charged leptons of type  $\alpha$  produced in either of the two scenarios considered is given by

$$\begin{aligned}
N(\alpha) = n_T \int_0^\infty dE \int_{q_{\min}}^{q_{\max}} dq \int_{-1}^{+1} d \cos \psi \int_{-1}^{+1} d \cos \xi \frac{1}{2\pi} \int_0^{2\pi} d\phi \\
\times \frac{d^2 F_\alpha(E, \xi)}{dE d \cos \xi} \cdot \frac{d^2 \sigma_\alpha(E, q, \cos \psi)}{dq d \cos \psi} \cdot P(\nu_\alpha \rightarrow \nu_\alpha; E, \xi).
\end{aligned} \tag{1}$$

Here  $d^2 F_\alpha/dE d \cos \xi$  is the differential flux of atmospheric neutrinos of type  $\nu_\alpha$  of energy  $E$  at zenith angle  $\xi$ . The term  $n_T$  is the effective number of target nucleons. The function  $d^2 \sigma_\alpha/dq d \cos \psi$  is the differential cross section for  $\nu_\alpha N \rightarrow \alpha X$  scattering, where  $q$  is the energy of the charged lepton and  $\psi$  is the scattering angle relative to the velocity vector of the incident  $\nu_\alpha$  (the azimuthal angle having been integrated over). The function  $P(\nu_\alpha \rightarrow \nu_\alpha; E, \xi)$  is the survival probability for a  $\nu_\alpha$  with energy  $E$  after travelling a distance  $L = \sqrt{(R+h)^2 - R^2 \sin^2 \xi} - R \cos \xi$ , where  $R$  is the radius of the Earth and  $h \sim 15$  km is the mean altitude at which atmospheric neutrinos are produced. Finally note that  $\phi$  is the azimuthal angle relative to the incident neutrino direction (see Fig.1 for an illustration of all the relevant angles). The integration over  $\phi$  is only non-trivial when calculating zenith angle binned data. In order to calculate the number of  $\alpha$ -like events for certain energy ranges and within certain zenith angle bins, the integration ranges in Eq.(1) must be truncated accordingly, with the direction of the charged lepton then obtained from

$$\cos \Theta = \cos \xi \cos \psi + \sin \xi \cos \phi \sin \psi, \tag{2}$$

where  $\Theta$  is the zenith angle of the charged lepton.

Since not all charged current events are used in the SuperKamiokande analysis, Eq.1 must be modified to incorporate the so-called detection efficiency function. This function is defined by

$$\text{detection efficiency} \equiv \frac{\text{Number of 1 ring charged current events}}{\text{Total number of charged current events}}. \tag{3}$$

For our sub-GeV analysis we use the approximation of only including quasi-elastic scattering. In this approximation the detection efficiency function is set to 1 because quasi-elastic scattering always lead to 1 ring events. In the multi-GeV analysis, we use a detection efficiency function obtained from the SuperKamiokande collaboration.

The survival probability  $P(\nu_\alpha \rightarrow \nu_\alpha; E, \xi)$  is obtained by solving the Schrödinger equation for neutrino evolution including matter effects. It is given by

$$i \frac{d}{dx} \begin{bmatrix} \nu_\mu(x) \\ \nu_{\tau,s}(x) \end{bmatrix} = \begin{bmatrix} \frac{\Delta m^2}{2E} \sin^2 \theta & \frac{\Delta m^2}{2E} \sin \theta \cos \theta \\ \frac{\Delta m^2}{2E} \sin \theta \cos \theta & \frac{\Delta m^2}{2E} \cos^2 \theta + A_{\tau,s}(x) \end{bmatrix} \begin{bmatrix} \nu_\mu(x) \\ \nu_{\tau,s}(x) \end{bmatrix}, \tag{4}$$

where  $x$  is the distance travelled,  $\Delta m^2$  the difference in squared masses,  $\theta$  the vacuum mixing angle and  $\nu_{\mu,\tau,s}(x)$  the wave-functions of the neutrinos. The quantities  $A_{\tau,s}(x)$  are the effective potential differences generated through the matter effect:

$$A_\tau(x) = 0 \tag{5}$$

and, for electrically neutral terrestrial matter [12]

$$A_s(x) = \frac{\sqrt{2}}{2}G_F N_n(x) = \frac{\sqrt{2}}{2}G_F(Y_n/m_n)\rho(x), \quad (6)$$

where  $G_F$  is the Fermi constant,  $N_n(x)$  is the number density of neutrons along the path of the neutrino,  $Y_n \simeq 0.52$  is the average number of neutrons per nucleon,  $m_n$  is the nucleon mass and  $\rho(x)$  is the mass density. Our numerical calculations use the density profile of the Earth given in Ref. [13]. The  $\nu_\mu$  survival probability is given by  $\nu_\mu(L)^*\nu_\mu(L)$ . For antineutrinos the sign of  $A_s$  is reversed.

The differential flux of atmospheric neutrinos  $d^2F_\alpha/dEd \cos \xi$  without geomagnetic effects is given in [16], but we have used the differential flux which includes geomagnetic effects [17]. (For other atmospheric neutrino flux calculations, see Ref. [18].)

SuperKamiokande separates its data into a sub-GeV sample and a multi-GeV sample. For sub-GeV events, charged leptons are dominantly produced via quasi-elastic scattering:  $\nu_\alpha N \rightarrow \alpha N'$ , where  $N$  and  $N'$  are nucleons. The state  $X$  [see Eq.(1)] is therefore identified with  $N'$  for these events. We use the cross-section given in Ref. [14]. The struck nucleon  $N$  is either a proton in hydrogen, or a bound nucleon in oxygen. In the case of hydrogen, the 2-body nature of quasi-elastic scattering leads to a relation between  $E$ ,  $q$  and  $\psi$  from relativistic energy-momentum conservation. One of the integrations in Eq.(1) is therefore redundant for scattering off hydrogen. For scattering off a nucleon within an oxygen nucleus, Fermi motion and Pauli blocking effects are incorporated via the prescription in Ref. [14]. In this case, there is no relation between  $E$ ,  $q$  and  $\psi$  because of the nuclear effects. For, multi-GeV events we use the inclusive cross-section for  $\nu_\alpha N \rightarrow \alpha X$  given in Ref. [15]. Although this cross section is not completely satisfactory for calculating absolute event rates because it does not incorporate low  $Q^2$  effects such as  $\Delta$  resonance production, it is a good enough approximation for calculating ratios of event rates such as up-down asymmetries [19] and  $N(\mu)/N(e)$  because these quantities are relatively insensitive to details. Indeed the main advantage in using event rate ratios is that they are relatively insensitive to uncertainties in the cross-sections and the neutrino fluxes. In this way 20 – 30% uncertainties in overall flux normalisations and cross-sections are avoided in favour of quantities with systematic uncertainties of only a few percent.

We will now define the event rate ratios used in the analysis. We first define the traditional quantity  $R$ , where

$$R \equiv \frac{(N_\mu/N_e)|_{osc}}{(N_\mu/N_e)|_{no-osc}}. \quad (7)$$

The quantities  $N_{e,\mu}$  are the numbers of  $e$ -like and  $\mu$ -like events, as per Eq.(1). The numerator denotes numbers obtained from Eq.(1), while the denominator the numbers expected with oscillations switched off. A class of up-down flux asymmetries for  $\alpha$ -like events is defined by

$$Y_\alpha^\eta \equiv \frac{(N_\alpha^{-\eta}/N_\alpha^{+\eta})|_{osc}}{(N_\alpha^{-\eta}/N_\alpha^{+\eta})|_{no-osc}}. \quad (8)$$

Here  $N_\alpha^{-\eta}$  denotes the number of  $\alpha$ -like events produced in the detector with zenith angle  $\cos \Theta < -\eta$ , while  $N_\alpha^{+\eta}$  denotes the analogous quantity for  $\cos \Theta > \eta$ , where  $\eta$  is defined to be positive. SuperKamiokande divides the  $(-1, +1)$  interval in  $\cos \Theta$  into five equal bins.

The central bin straddles both the upper and lower hemispheres, and is thus not useful for up-down asymmetry analyses. We therefore choose  $\eta = 0.2$  in order to utilise all the data in the other four bins. Since  $\nu_e$ 's do not oscillate in the two scenarios  $\nu_\mu \rightarrow \nu_{\tau,s}$  which we consider, up-down asymmetries for  $e$ -like events,  $Y_e^{0.2}$  are predicted to equal 1. Note that systematic uncertainties for up-down asymmetries are smaller than for  $R$ , because the latter depends on the relative flux of  $\nu_\mu$  to  $\nu_e$ .

In the context of the  $\nu_\mu \rightarrow \nu_{\tau,s}$  scenarios considered here,  $R$  measures the disappearance of  $\nu_\mu$ 's and  $\bar{\nu}_\mu$ 's relative to  $\nu_e$ 's and  $\bar{\nu}_e$ 's and to no-oscillation expectations. The up-down asymmetries probe the zenith angle dependences of the neutrino fluxes relative to no-oscillation expectations. Both classes of quantities provide pertinent information about the pattern of the putative  $\nu_\mu$  oscillations while being insensitive to the systematic uncertainties discussed above.

Additional important information about the oscillation pattern is supplied by the energy dependences of  $R$  and the  $Y$ 's. For this reason we calculate separate  $R$ 's and  $Y$ 's for the SuperKamiokande sub-GeV and multi-GeV samples. The sub-GeV sample is defined by the momentum cuts  $0.1 < p_e/GeV < 1.33$  and  $0.2 < p_\mu/GeV < 1.5$  for  $e$ -like and  $\mu$ -like events, respectively. We also consider an alternative low-energy cut which has a lower limit of 0.5 GeV. The alternative cut enhances the effect of oscillations because the correlation of the produced charged leptons with the incident neutrinos is stronger for higher energies.

Our results for the  $R$ 's and  $Y$ 's are displayed in Figs.2-6 [20] together with the preliminary SuperKamiokande results [2],

$$\begin{aligned}
R(sub - GeV) &= 0.61 \pm 0.03 \pm 0.05, \\
R(multi - GeV) &= 0.67 \pm 0.06 \pm 0.08, \\
Y_\mu^{0.2}(sub - GeV) &= 0.78 \pm 0.06, \\
Y_\mu^{0.2}(multi - GeV) &= 0.49 \pm 0.06.
\end{aligned}
\tag{9}$$

The preliminary experimental results we use correspond to 414 live days of running. Note that experimental results for the alternative sub-GeV sample with  $p_{e,\mu} > 0.5$  GeV are not at present available. For completeness we mention that the preliminary SuperKamiokande results for the  $e$ -like up-down asymmetries are

$$\begin{aligned}
Y_e^{0.2}(sub - GeV) &= 1.13 \pm 0.08, \\
Y_e^{0.2}(multi - GeV) &= 0.83 \pm 0.13.
\end{aligned}
\tag{10}$$

Finally note that only statistical errors are given for the up-down asymmetries since they should be much larger than possible systematic errors.

These results have several significant features: (i) For the sub-GeV cases, the matter effects become noticeable at about  $\Delta m^2 = 10^{-3}$  eV<sup>2</sup> and are really very significant at  $\Delta m^2 = 10^{-4}$  eV<sup>2</sup>. (ii) The matter effects cut in at the higher value of about  $\Delta m^2 = 10^{-2}$  eV<sup>2</sup> for the multi-GeV cases. (iii) The up-down muon asymmetries plateau between about  $10^{-3}$  and  $10^{-2}$  eV<sup>2</sup>, with the sub-GeV plateau occurring for slightly lower values of  $\Delta m^2$  compared to the multi-GeV case. For this range of  $\Delta m^2$ , downward travelling neutrinos do not have time to oscillate, whereas upward travelling neutrinos experience averaged oscillations. The plateau phenomenon provides a characteristic prediction for up-down asymmetries that is

reasonably insensitive to  $\Delta m^2$ , while remaining sensitive to the mixing angle. Note also that the multi-GeV  $R$  flattens out in this  $\Delta m^2$  range, for exactly the same reason, with the corresponding plateau for the sub-GeV  $R$  at lower  $\Delta m^2$ 's (except that the matter effect destroys the plateau for the  $\nu_\mu - \nu_s$  scenario). (iv) Both the sub- and multi-GeV  $Y$ 's fit the SuperKamiokande data well for  $\Delta m^2$  in the range  $10^{-3} - 10^{-2}$  eV<sup>2</sup>. The  $R$  values also fit the data well in this range, but with a preference for higher  $\Delta m^2$  values. (v) While a fairly large range of mixing angle values is consistent with both of the  $R$  measurements and the sub-GeV  $Y$  datum, the multi-GeV  $Y$  result tends to favour maximal mixing. The multi-GeV  $R$  measurement also tends to favour a large mixing angle. (vi) A comparison of Figs.4 and 5 shows that the alternative low-energy cut increases both the up-down asymmetry effect and the matter effect.

We now perform a  $\chi^2$  fit to these data in order to quantify the significance of the various competing influences discussed above. We define the  $\chi^2$  function as

$$\chi^2 = \sum_E \left[ \left( \frac{R^{SK} - R^{th}}{\delta R^{SK}} \right)^2 + \left( \frac{Y_\mu^{SK} - Y_\mu^{th}}{\delta Y_\mu^{SK}} \right)^2 + \left( \frac{Y_e^{SK} - Y_e^{th}}{\delta Y_e^{SK}} \right)^2 \right], \quad (11)$$

where the sum is over the sub-GeV and multi-GeV cases, the measured SuperKamiokande values and errors are denoted by the superscript ‘‘SK’’ and the theoretical predictions for the quantities are labelled by ‘‘th’’. The  $\eta = 0.2$  choice is understood for the up-down asymmetries. We include both the  $e$ -like and the  $\mu$ -like up-down asymmetries in the fit. There are 6 pieces of data in  $\chi^2$  and 2 adjustable parameters,  $\Delta m^2$  and  $\sin^2 2\theta$ , leaving 4 degrees of freedom.

The statistical procedure we employ is approximate in the sense that ratios of Gaussian-distributed quantities are only approximately Gaussian themselves [21]. The validity of using ratios increases as the fractional errors decrease. Since SuperKamiokande is a high statistics experiment, our procedure is accurate within a sufficiently small region around the best fit point provided this point gives a good fit (we estimate that it is approximately valid within the  $3\sigma$  region around the best fit).

An alternative  $\chi^2$  analysis can be performed by using absolute event rates rather than ratios. However in that case the numerical validity of the results is limited by the correctness of the cross-sections used. These analyses typically incorporate a 20 – 30% uncertainty in the event rates due to uncertain fluxes by introducing theoretical errors in addition to measurement errors. Unfortunately, existing analyses do not address the issue of uncertain cross-sections. Our analysis avoids this problem, and is therefore complementary to the absolute event rate type of analysis. Our work also extends other recent fits [2,22] by considering the  $\nu_\mu \rightarrow \nu_s$  case.

The results of the  $\chi^2$  fits are displayed in Figs.7-12. Figure 7 shows the allowed region of  $(\sin^2 2\theta, \Delta m^2)$  at various confidence levels for the  $\nu_\mu \rightarrow \nu_\tau$  scenario. Maximal mixing provides the best fit, and  $\Delta m^2$  values in the  $10^{-3}$  to  $10^{-2}$  eV<sup>2</sup> range are favoured. Note that the confidence levels are defined in the usual way by

$$\chi^2 = \chi_{min}^2 + \Delta\chi^2 \quad (12)$$

where  $\Delta\chi^2 = 2.3, 4.6, 6.2, 11.8$  for the  $1\sigma, 90\%$  C.L.,  $2\sigma$  and  $3\sigma$  allowed region respectively. Our  $\chi_{min}^2$  for  $\nu_\mu \rightarrow \nu_\tau$  oscillations is  $\chi_{min}^2 = 4.5$  for 4 degrees of freedom. This is quite a good fit to the data (allowed at the 35% level).

In Figure 8 we show the allowed region considering just the asymmetries instead of using both the asymmetries and the  $R$  ratios. This is of interest because systematic uncertainties for  $Y$ 's are smaller than those for  $R$ 's. Note that in this case there are 4 data points and 2 free parameters which gives 2 degrees of freedom.

According to Fig.9,  $\chi^2$  does not experience a deep minimum at the best fit point with respect to  $\Delta m^2$ . This reflects the plateau phenomenon discussed earlier, and shows that this type of atmospheric neutrino analysis will not be able to pinpoint  $\Delta m^2$  very precisely. Note that the minimum becomes shallower when the  $R$ 's are excluded from the fit. This is because the plateau in  $R$  is not as pronounced as that in  $Y$ .

Figures 10-12 show the corresponding results for the  $\nu_\mu \rightarrow \nu_s$  scenario. Smaller values of  $\Delta m^2$  are disfavoured in this case because the matter effect moves both  $R$  and  $Y$  away from the measured values. However, an order of magnitude spread in  $\Delta m^2$  is nonetheless permitted at the  $3\sigma$  level. It is interesting to note that present data tend to predict a positive signal for future long baseline experiments for the  $\nu_\mu \rightarrow \nu_s$  scenario, whereas the  $\nu_\mu \rightarrow \nu_\tau$  scenario permits  $\Delta m^2$  values that are too small to be probed in this manner. The value of  $\chi_{min}^2$  for the  $\nu_\mu \rightarrow \nu_s$  scenario is  $\chi_{min}^2 = 5.1$  for 4 degrees of freedom. This is similar to  $\nu_\mu - \nu_\tau$  case and also represents quite a good fit (which is allowed at 28%).

In conclusion, we have demonstrated that matter effects in the Earth have a significant role to play in comparing and contrasting the  $\nu_\mu \rightarrow \nu_\tau$  and  $\nu_\mu \rightarrow \nu_s$  solutions to the atmospheric neutrino anomaly with SuperKamiokande data. The matter effects increase both the ratio of  $\mu$ -like to  $e$ -like events, and  $\mu$ -type up-down asymmetries, for the  $\nu_\mu \rightarrow \nu_s$  case relative to the  $\nu_\mu \rightarrow \nu_\tau$  case for sufficiently small values of  $\Delta m^2$  ( $< 10^{-2}$  and  $< 10^{-3}$  eV<sup>2</sup> for the multi-GeV and sub-GeV samples, respectively). Smaller  $\Delta m^2$  values ( $\lesssim 2 \times 10^{-3}$  eV<sup>2</sup>) are disfavoured for the  $\nu_\mu \rightarrow \nu_s$  scenario, with interesting implications for future long baseline experiments.

## ACKNOWLEDGMENTS

O.Y. would like to acknowledge the hospitality of the School of Physics at The University of Melbourne where this work was done. O.Y. was supported in part by a Grant-in-Aid for Scientific Research of the Ministry of Education, Science and Culture, #09045036. O.Y. would like to thank T. Kajita for useful communications and the participants of the Neutrino Symposium at Hachimantai, Japan, on Nov.28-30 1997 for discussions. R.F. and R.R.V. are supported by the Australian Research Council.

## REFERENCES

- [1] Kamiokande Collaboration, K.S. Hirata et al., Phys. Lett. **B205**, 416 (1988); *ibid.* **B280**, 146 (1992); Kamiokande Collaboration, Y. Fukuda et al., Phys. Lett. **B335**, 237 (1994); IMB Collaboration, D. Casper et al., Phys. Rev. Lett. **66**, 2561 (1989); R. Becker-Szendy et al., Phys. Rev. **D46**, 3720 (1989); NUSEX Collaboration, M. Aglietta et al., Europhys. Lett. **8**, 611 (1989); Frejus Collaboration, Ch. Berger et al., Phys. Lett. **B227**, 489 (1989); *ibid.* **B245**, 305 (1990); K. Daum et al., Z. Phys. **C66** 417 (1995); Soudan 2 Collaboration, M. Goodman et al., Nucl. Phys. **B** (Proc. Suppl.) **38,337** (1995); W.W.M., Allison et. al., Phys. Lett. **B391**, 491 (1997).
- [2] E. Kearns, Talk at *News about SNUS*, ITP Workshop, Santa Barbara, Dec. 1997, <http://doug-pc.itp.ucsb.edu/online/snu/kearns/oh/all.html>.
- [3] A. Acker and S. Pakvasa, Phys. Lett. **B397**, 209 (1997); A. Acker, S. Pakvasa, J. Learned and T. J. Weiler, Phys. Lett. **B298**, 149 (1993).
- [4] J. G. Learned, S. Pakvasa and T. J. Weiler, Phys. Lett. **B207**, 79 (1988); V. Barger and K. Whisnant, Phys. Lett. **B209**, 365 (1988); K. Hidaka, M. Honda and S. Midorikawa, Phys. Rev. Lett. **61**, 1537 (1988); J. T. Peltoniemi and J. W. F. Valle, Nucl. Phys. **B406**, 409 (1993); D. O. Caldwell and R. N. Mohapatra, Phys. Rev. **D50**, 3477 (1994); C. Y. Cardall and G. Fuller, Phys. Rev. **D53**, 4421 (1996).
- [5] E. Akhmedov, P. Lipari and M. Lusignoli, Phys. Lett. **B300**, 128 (1993); R. Foot, Mod. Phys. Lett. **A9**, 169 (1994); R. Foot and R. R. Volkas, Phys. Rev. **D52**, 6595 (1995); Q. Y. Liu and A. Yu. Smirnov, hep-ph/9712493. Note that the implications of the  $\nu_\mu - \nu_s$  solution for Big Bang Nucleosynthesis for the case of maximal mixing are studied in R. Foot and R. R. Volkas, Phys. Rev. **D55**, 5147 (1997); Astropart. Phys. **7**, 283 (1997); Phys. Rev. **D56**, 6653 (1997). For other models with large angle or maximal active-sterile mixing see, for instance, M. Kobayashi, C. S. Lim and M. M. Nojiri, Phys. Rev. Lett. **67**, 1685 (1991); C. Giunti, C. W. Kim and U. W. Lee, Phys. Rev. **D46**, 3034 (1992); J. Bowes and R. R. Volkas, University of Melbourne Preprint UM-P-97/09.
- [6] In this paper we focus on 2 flavour oscillations. For 3 flavour analyses of the atmospheric neutrino problem see, for example, O. Yasuda, TMUP-HEL-9706, hep-ph/9706546; S. M. Bilenky, C. Giunti and C. W. Kim, Astropart. Phys. **4**, 241 (1996); G. L. Fogli, E. Lisi, D. Montanino and G. Scioscia, Phys. Rev. **D55**, 4385 (1997); M. Narayan, G. Rajasekaran and S. Uma Sankar, Phys. Rev. **D56**, 437 (1997); P. H. Harrison, D. Perkins and W. G. Scott, Phys. Lett. **B396**, 186 (1997); **B349**, 137 (1995).
- [7] CHOOZ Collaboration, M. Apollonio et al., hep-ex/9711002.
- [8] L. Wolfenstein, Phys. Rev. **D17**, 2369 (1978); S. P. Mikheyev and A. Yu Smirnov, Yad. Fiz. **42**, 1441 (1985) [Sov. J. Nucl. Phys. **42**, 913 (1985)]; Nuovo Cim. **C9**, 17 (1986).
- [9] T. Kajita, Talk at *Topical Workshop on Neutrino Physics*, Institute for Theoretical Physics, The University of Adelaide, Nov. 1996; F. Vissani and A. Yu Smirnov, hep-ph/9710565.
- [10] See the paper by Liu and Smirnov in Ref. [5].
- [11] F. Ronga, *Proceedings of the 17th International Conference on Neutrino Physics and Astrophysics* (World Scientific, Singapore, 1997), eds. K. Enqvist et al., p.529.
- [12] See for example, D. Notzold and G. Raffelt, Nucl. Phys. **B307**, 924 (1988).
- [13] F. Stacey, *Physics of the Earth, 2nd ed.* (J. Wiley and Sons, Chichester, 1977).



- [14] T. K. Gaisser and J. S. O'Connell, Phys. Rev. **D34**, 822 (1986).
- [15] V. Barger and R. J. N. Phillips, *Collider Physics* (Addison-Wesley, Redwood City, 1987), p.153.
- [16] M. Honda, T. Kajita, S. Midorikawa, and K. Kasahara, Phys. Rev. **D52**, 4985 (1995).
- [17] M. Honda, K. Kasahara, and S. Midorikawa, private communication.
- [18] L.V. Volkova, Sov. J. Nucl. Phys. **31**, 784 (1980); T.K. Gaisser, T. Stanev S.A. Bludman and H. Lee, Phys. Rev. Lett. **51**, 223 (1983); A. Dar, Phys. Rev. Lett. **51**, 227 (1983); K. Mitsui, Y. Minorikawa and H. Komori, Nuovo Cim. **C9**, 995 (1986); E.V. Bugaev and V.A. Naumov, Sov. J. Nucl. Phys. **45**, 857 (1987); T.K. Gaisser, T. Stanev and G. Bar, Phys. Rev. **D38**, 85 (1988); A.V. Butkevich, L.G. Dedenko and I.M. Zheleznykh, Sov. J. Nucl. Phys. **50**, 90 (1989); M. Honda, K. Kasahara, K. Hidaka and S. Midorikawa, Phys. Lett. **B248**, 193 (1990); H. Lee and Y. S. Koh, Nuovo Cim. **B105**, 883 (1990); M. Kawasaki and S. Mizuta, Phys. Rev. **D43**, 2900 (1991); P. Lipari, Astropart. Phys. **1**, 195 (1993). D.H. Perkins, Astropart. Phys. **2**, 249 (1994); V. Agrawal, T.K. Gaisser, P. Lipari and T. Stanev, Phys. Rev. **D53**, 1314 (1996); T.K. Gaisser and T. Stanev, astro-ph/9708146.
- [19] J. Bunn, R. Foot and R. R. Volkas, Phys. Lett. **B413**, 109 (1997); J. W. Flanagan, J. G. Learned and S. Pakvasa, hep-ph/9709438; R. Foot, R. R. Volkas and O. Yasuda, hep-ph/9709483, Phys. Rev. **D** (in press); hep-ph/9710403, Phys. Lett. **B** (in press).
- [20] In our numerical work we found some small oscillations ( $\sim 5\%$ ) of the  $Y$  parameter which we have smoothed out in the Figures.
- [21] G. L. Fogli and E. Lisi, Phys. Rev. **D52**, 2775 (1995).
- [22] M. C. Gonzalez-Garcia et al., hep-ph/9801368.

## Figure Captions

Figure 1. The parameterisation of angles in the interaction  $\nu_\alpha N \rightarrow \alpha X$ .

Figure 2. The sub-GeV  $R$  as a function of  $\Delta m^2$  for various values of  $\sin^2 2\theta$ . The usual SuperKamiokande momentum cuts have been employed. The solid (dashed) lines pertain to the  $\nu_\mu \rightarrow \nu_\tau$  ( $\nu_\mu \rightarrow \nu_s$ ) scenario. Going from the top to the bottom curves,  $\sin^2 2\theta$  takes the values 0.7, 0.8, 0.9 and 1. Note the significance of the matter effect for  $\Delta m^2 < 10^{-3}$  eV<sup>2</sup>. The dashed-dotted lines denote the preliminary SuperKamiokande result within a  $\pm 1\sigma$  band after 414 live days of running.

Figure 3. The multi-GeV  $R$  as a function of  $\Delta m^2$ . Notation as for Fig.2. Note the significance of the matter effect for  $\Delta m^2 < 10^{-2}$  eV<sup>2</sup>.

Figure 4. The up-down  $\mu$ -type asymmetry  $Y_\mu^{0.2}$  as a function of  $\Delta m^2$  for the sub-GeV sample with the usual SuperKamiokande momentum cuts. Notation as for Fig.2, except that in the  $Y > 1$  region the order of the  $\sin^2 2\theta$  values is reversed. Note the significance of the matter effect for  $\Delta m^2 < 10^{-3}$  eV<sup>2</sup>.

Figure 5. The up-down  $\mu$ -type asymmetry  $Y_\mu^{0.2}$  as a function of  $\Delta m^2$  for the sub-GeV sample with the alternative lower limit  $p_\mu > 0.5$  GeV. Notation as for Fig.2, except that in the  $Y > 1$  region the order of the  $\sin^2 2\theta$  values is reversed. Note the significance of the matter effect for  $\Delta m^2 < 10^{-3}$  eV<sup>2</sup>.

Figure 6. The up-down  $\mu$ -type asymmetry  $Y_\mu^{0.2}$  as a function of  $\Delta m^2$  for the multi-GeV sample. Both fully-contained and partially-contained events are included. Notation as for Fig.2. Note the significance of the matter effect for  $\Delta m^2 < 10^{-2}$  eV<sup>2</sup>.

Figure 7. The allowed region in the  $(\sin^2 2\theta, \Delta m^2)$  plane for the  $\nu_\mu \rightarrow \nu_\tau$  scenario.

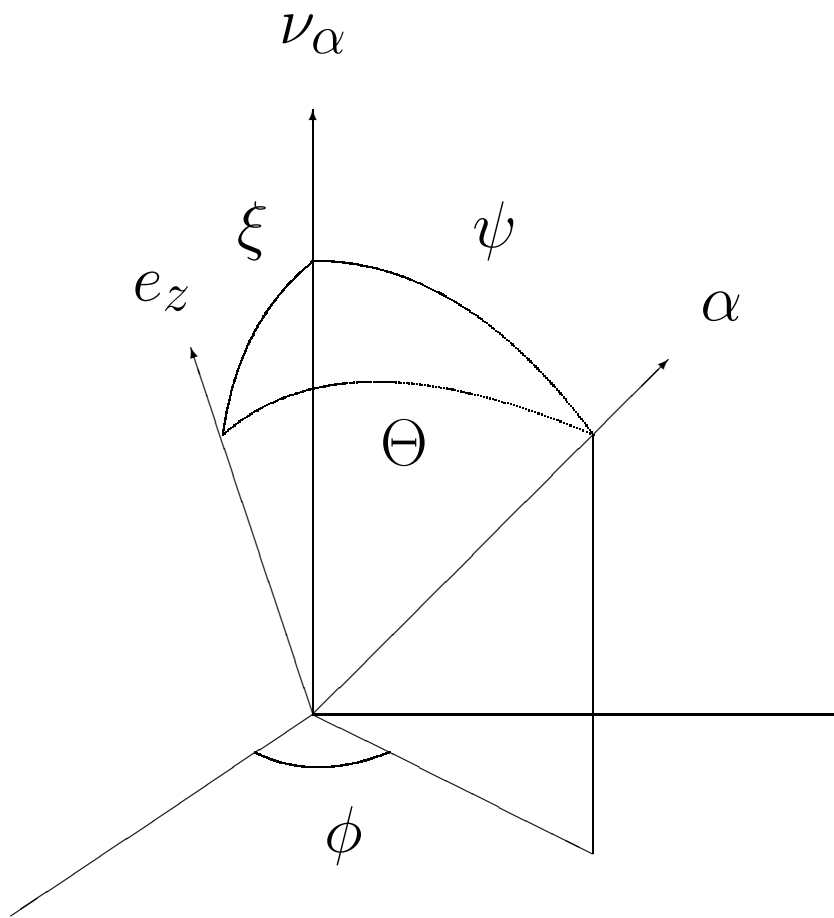
Figure 8. As for Fig.7 but with  $R$  data excluded from the fit.

Figure 9.  $\chi^2$  as a function of  $\Delta m^2$  along the  $\sin^2 2\theta = 1$  line for the  $\nu_\mu \rightarrow \nu_\tau$  scenario. Note the shallow minimum. Note also that the minimum becomes shallower still if  $R$  is excluded from the fit. The insensitivity to  $\Delta m^2$  corresponds to the plateau features in Figs.2-6 (see text).

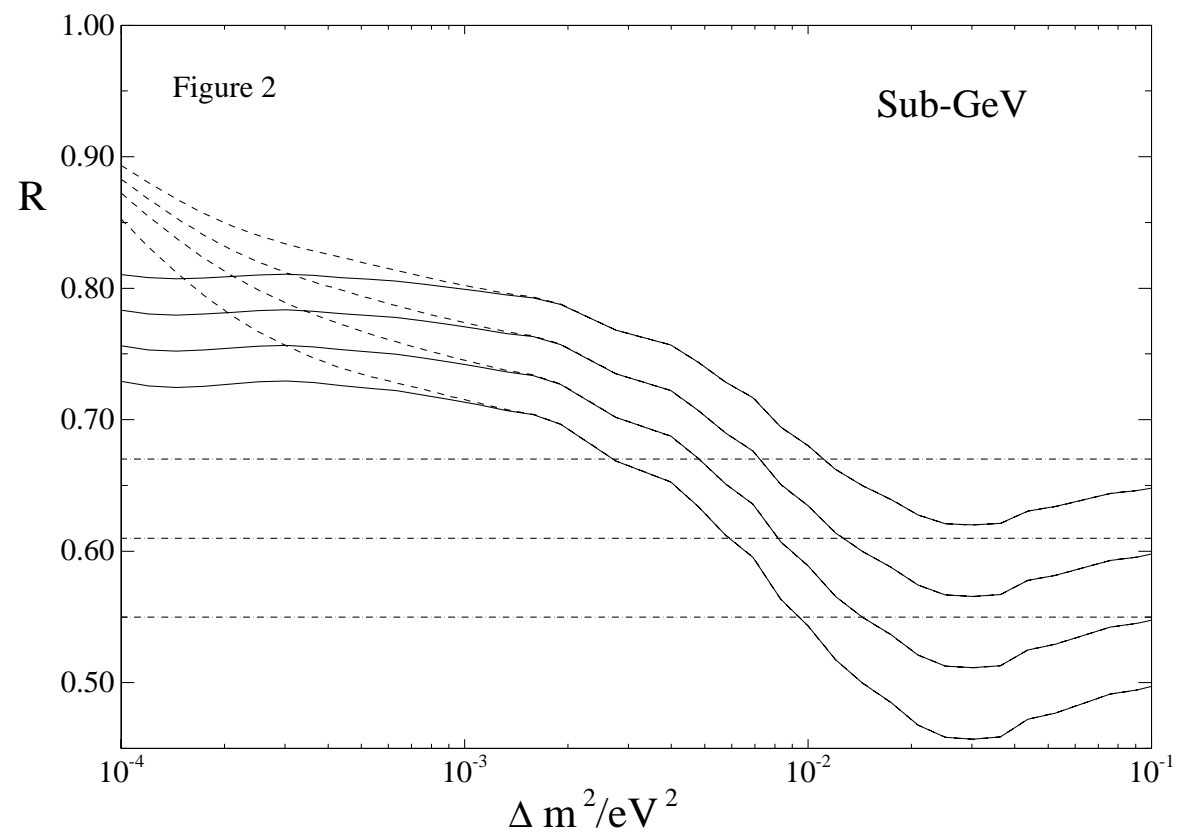
Figure 10. The allowed region in the  $(\sin^2 2\theta, \Delta m^2)$  plane for the  $\nu_\mu \rightarrow \nu_s$  scenario.

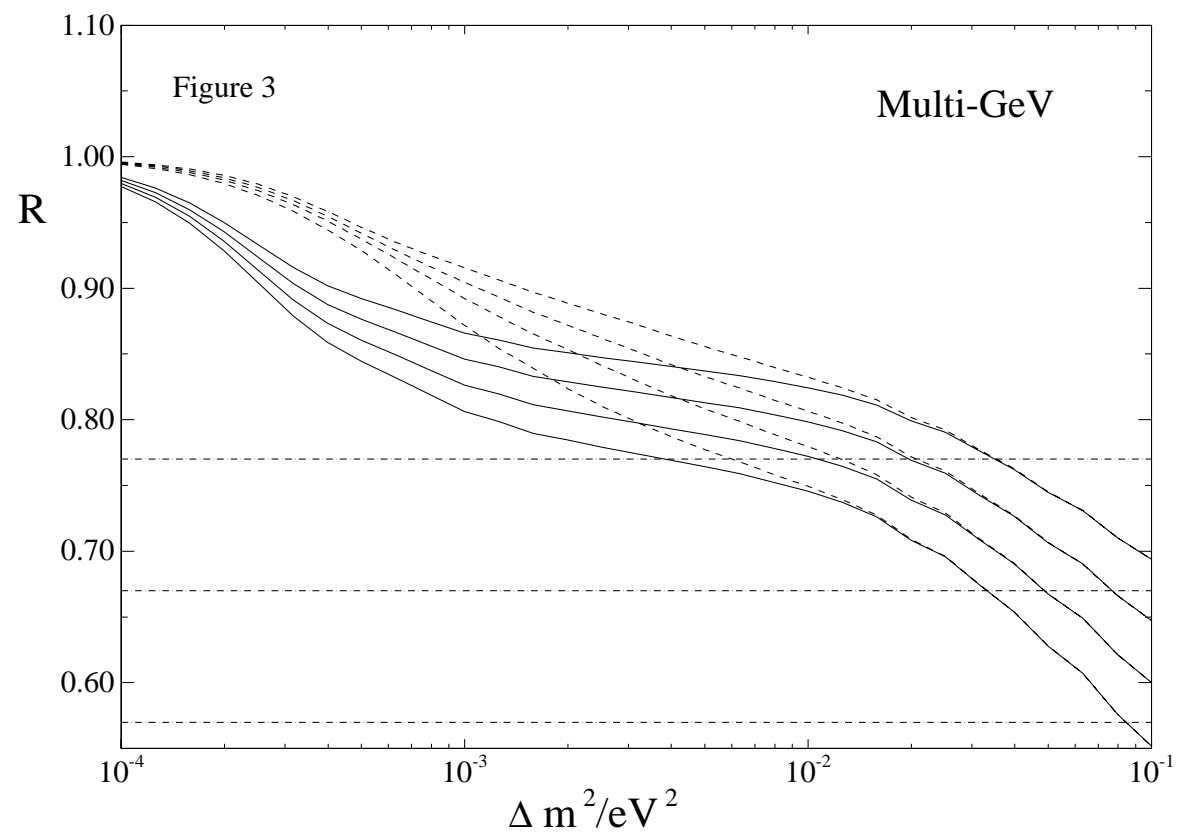
Figure 11. As for Figure 10 but with  $R$  data excluded from the fit.

Figure 12. As for Fig.9 but for the  $\nu_\mu \rightarrow \nu_s$  scenario.

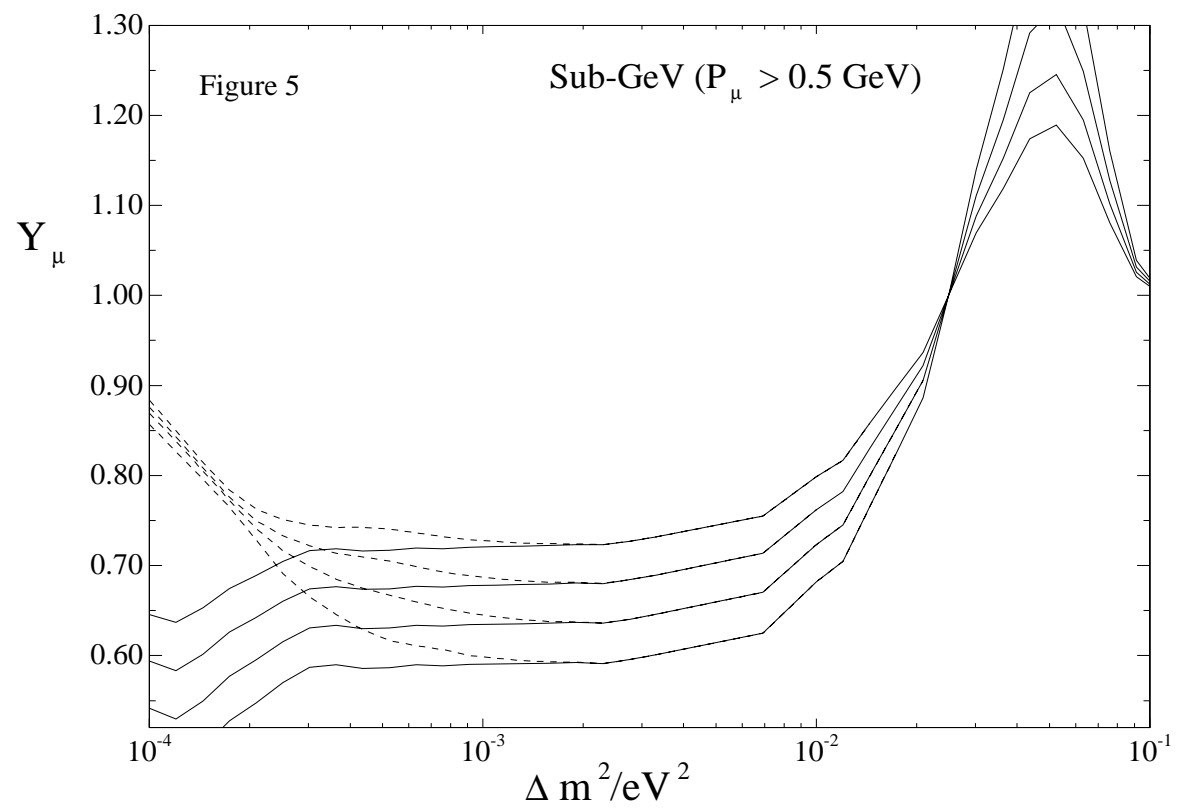


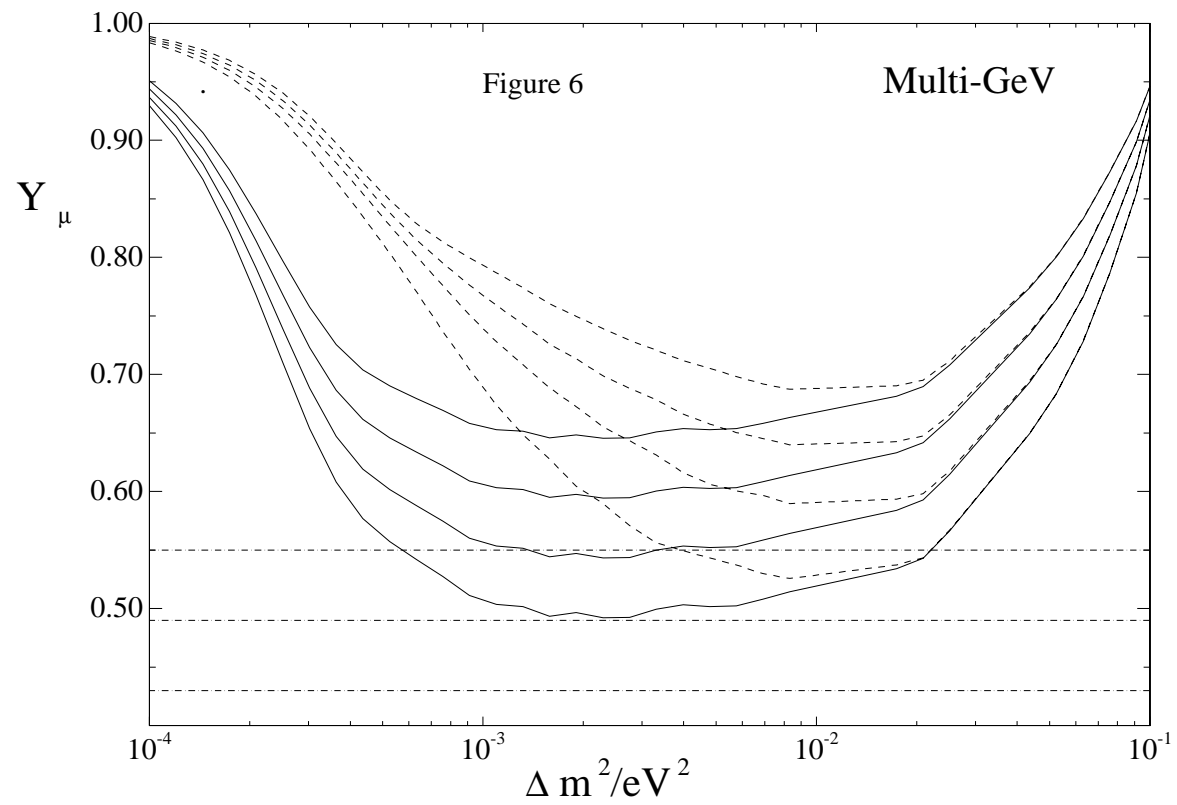
**Fig.1**













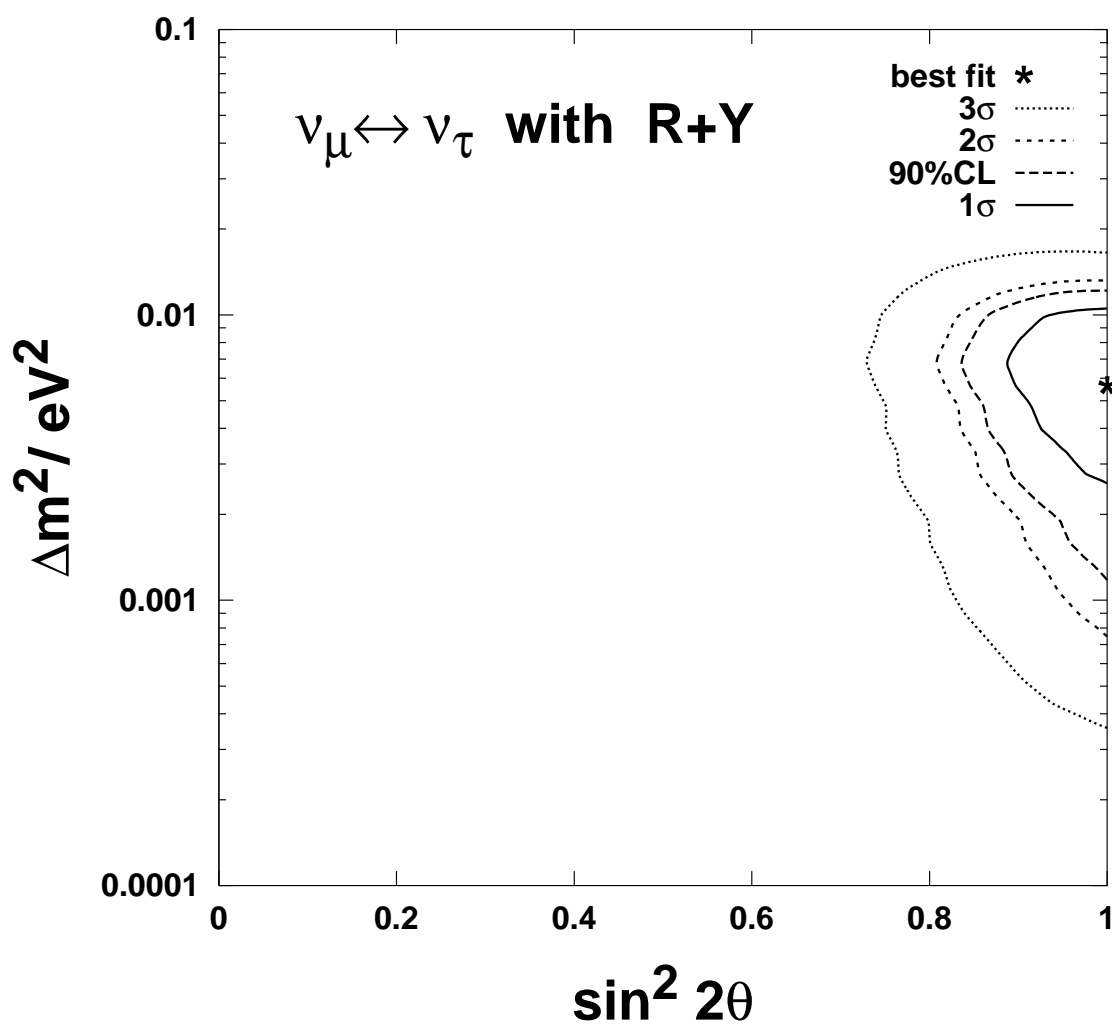


**Fig.7**

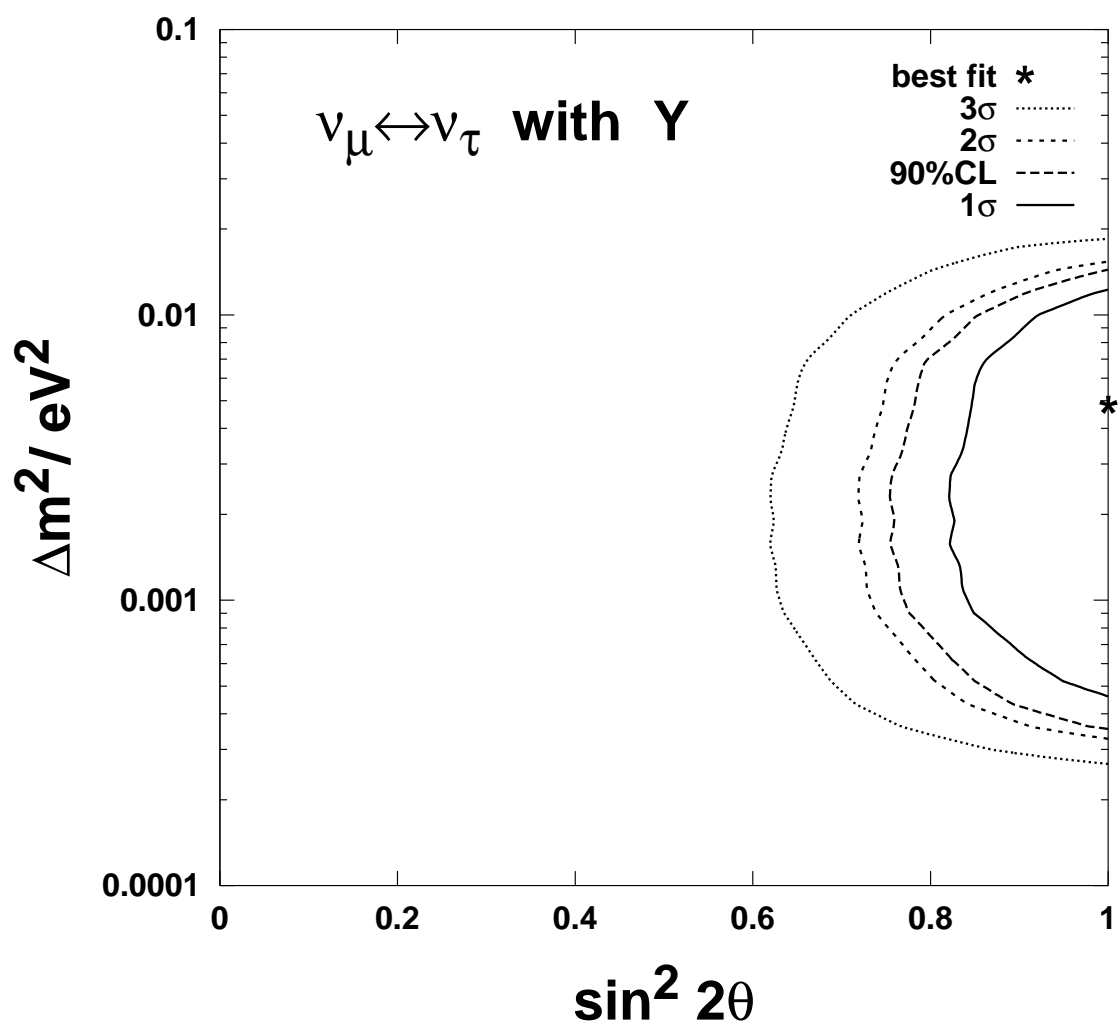


**Fig.8**

$\nu_\mu \leftrightarrow \nu_\tau, \sin^2 2\theta=1$

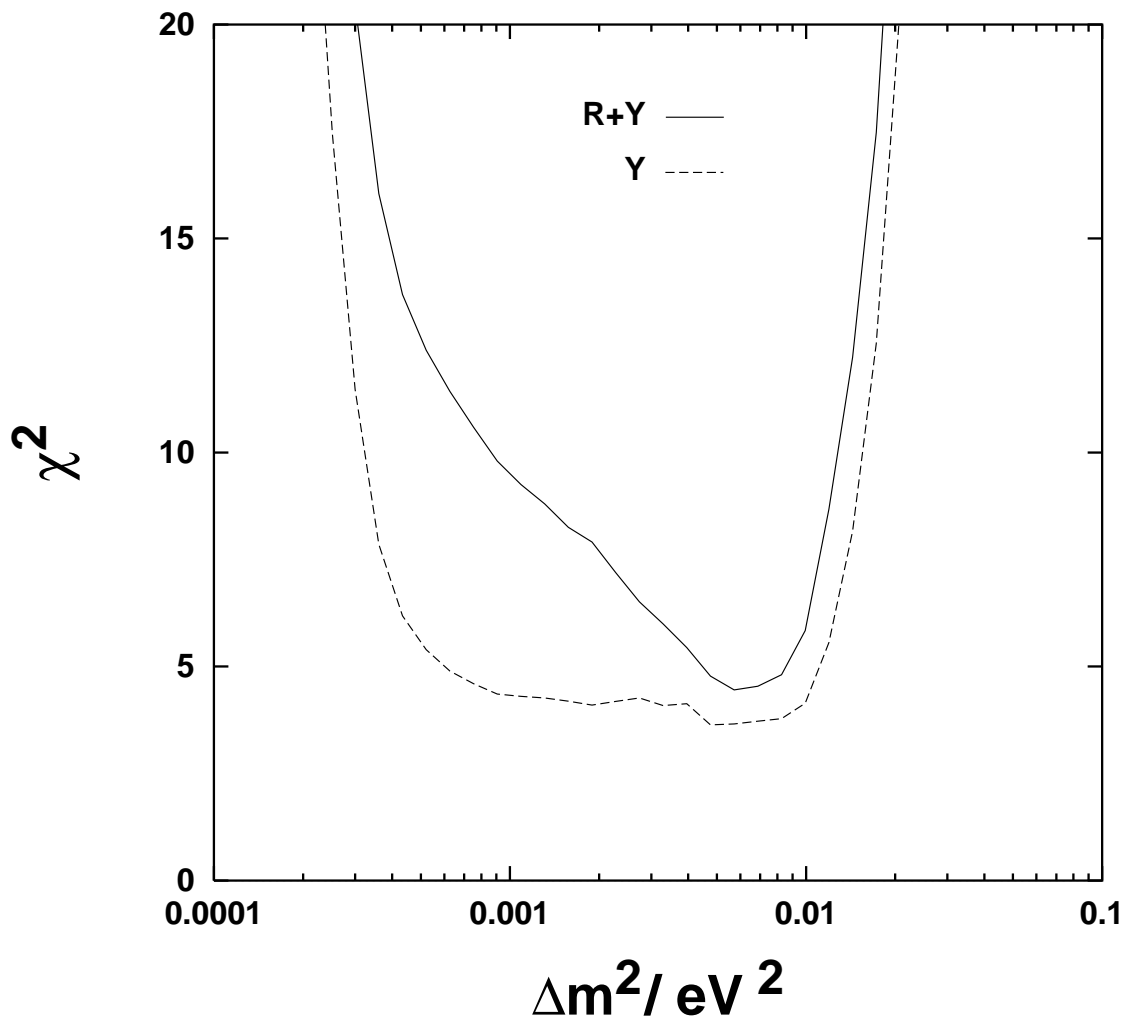


**Fig.9**

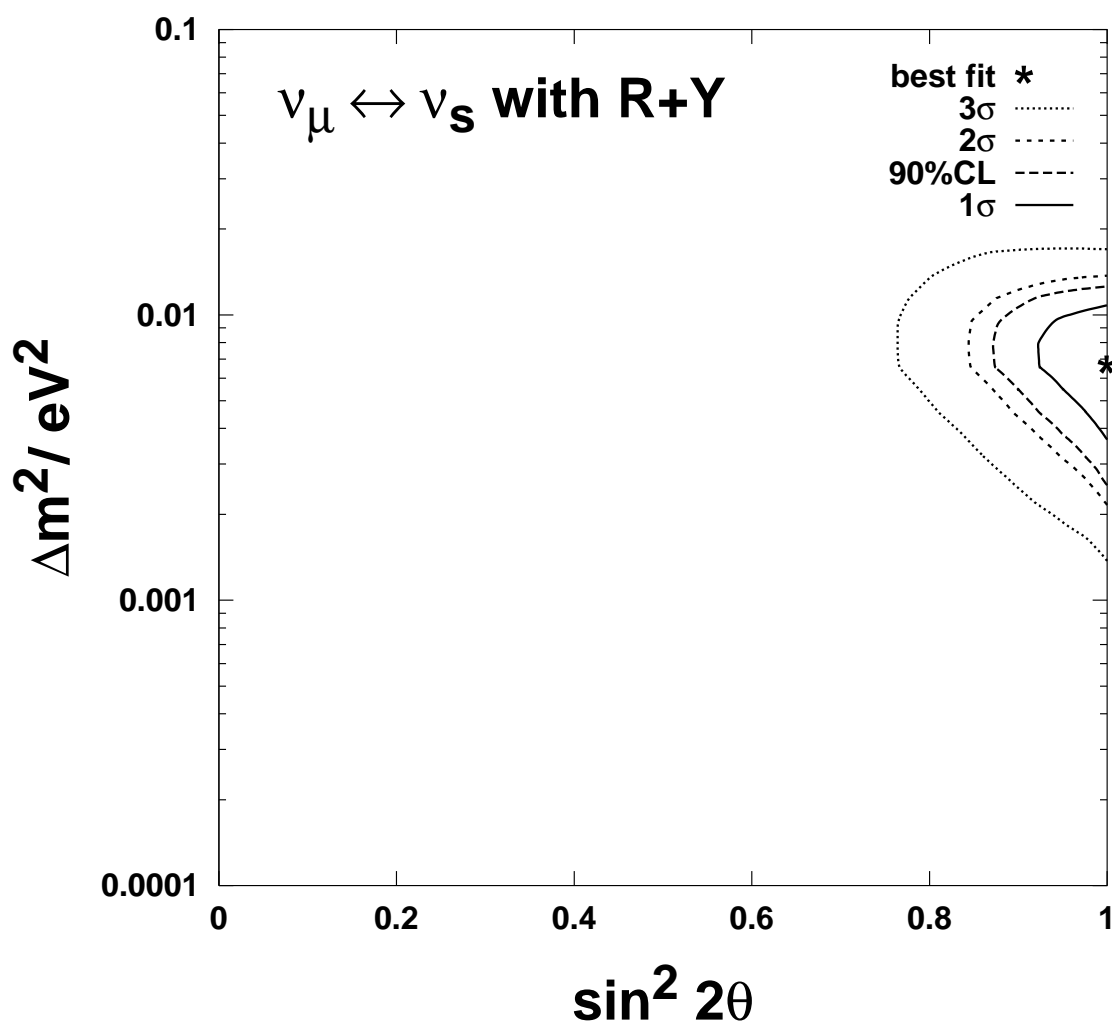


**Fig.10**

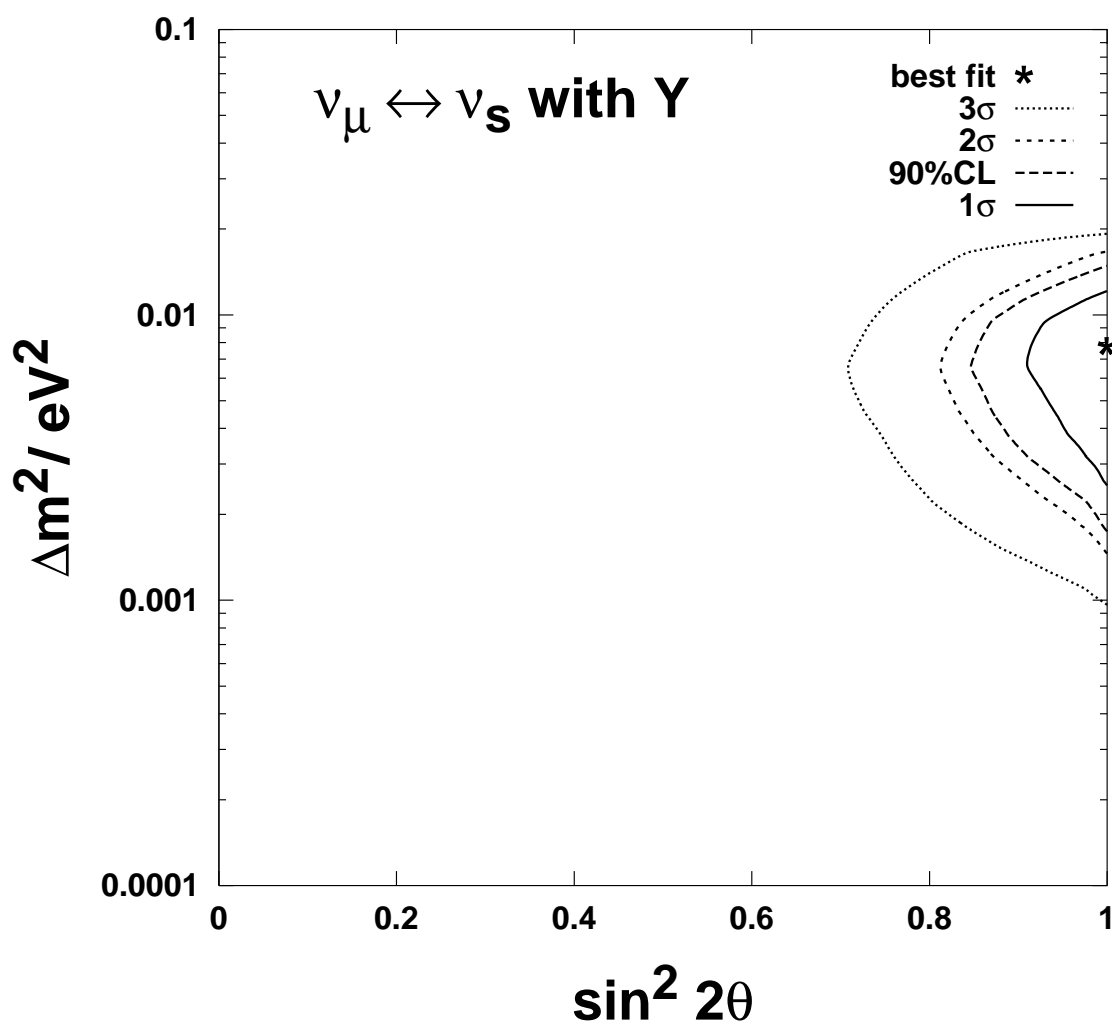


**Fig.11**

$\nu_\mu \leftrightarrow \nu_s, \sin^2 2\theta=1$

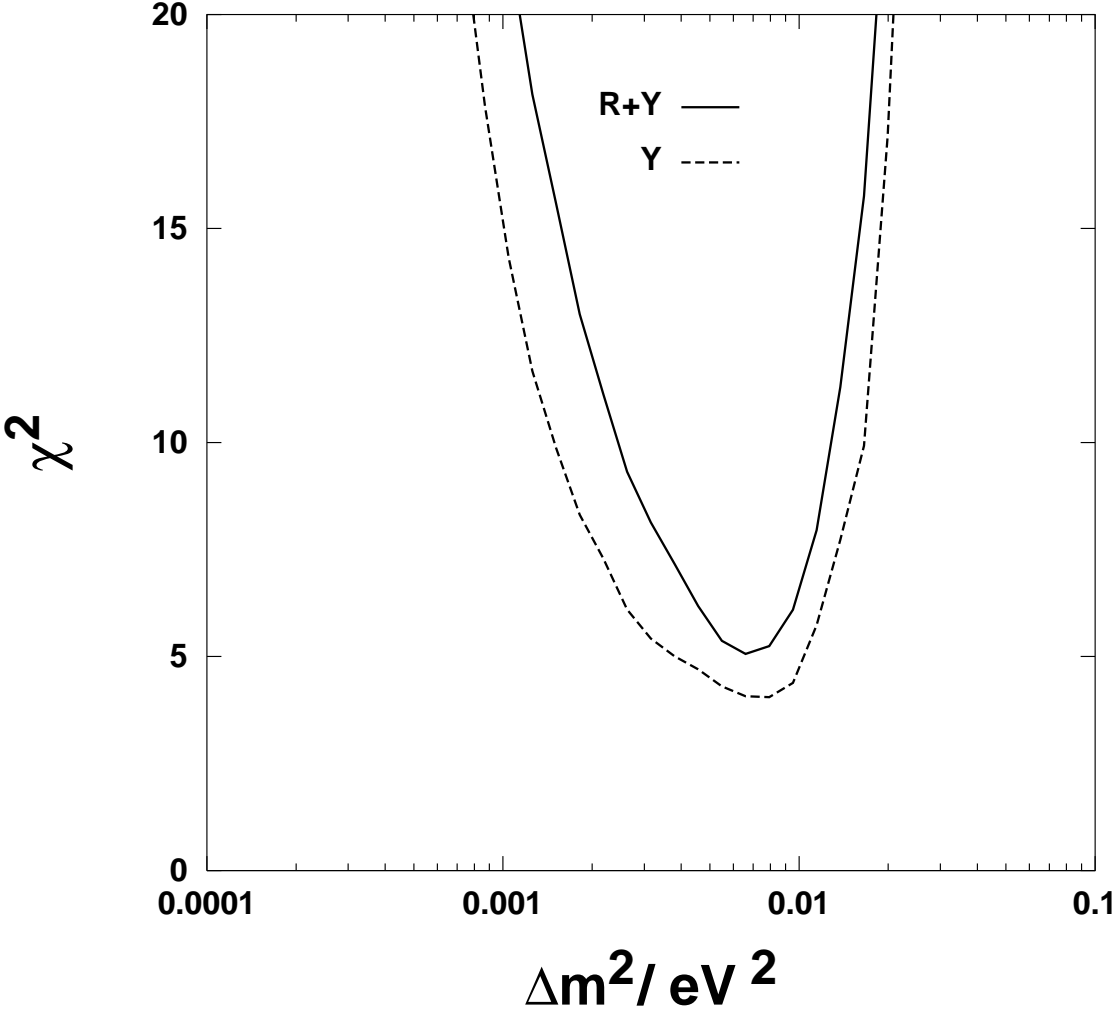


**Fig.12**